Orbital-Angular-Momentum Embedded Massive MIMO: Achieving Multiplicative Spectrum-Efficiency for mmWave Communications

WENCHI CHENG, (Member, IEEE), HAILIN ZHANG, (Member, IEEE),
LIPING LIANG, HAIYUE JING, AND ZAN LI, (Senior Member, IEEE)
State Key Laboratory of Integrated Services Networks, Xidian University, Xi'an 710071, China

Correponding author: Wenchi Cheng (wccheng@xidian.edu.cn)

ABSTRACT By enabling very high bandwidth for radio communications, the millimeter-wave (mmWave), which can easily be integrated with massive-multiple-input-multiple-output (massive-MIMO) due to small antenna size, has been attracting growing attention as a candidate for the fifth-generation (5G) and 5G-beyond wireless communications networks. On the other hand, the communication over the orthogonal states/modes of orbital angular momentum (OAM) is a subset of the solutions offered by massive-MIMO communications. Traditional massive-MIMO-based mmWave communications did not concern the potential spectrum-efficiency-gain (SE-gain) offered by the orthogonal states of OAM. However, the highly expected maximum SE-gain for OAM and massive-MIMO communications is the product of SE-gains offered by OAM and multiplexing-MIMO. In this paper, we propose the OAM-embedded-MIMO (OEM) communication framework to obtain the multiplicative SE-gain for joint OAM and massive-MIMO-based mmWave wireless communications. We design the parabolic antenna for each uniform circular array antenna to converge OAM signals. Then, we develop the mode-decomposition and multiplexing-detection scheme to obtain the transmit signal on each OAM-mode of each transmit antenna. Also, we develop the OEM-water-filling power allocation policy to achieve the maximum multiplicative SE-gain for OEM communications. The extensive simulations obtained validate and evaluate our developed a parabolic antenna-based converging method, a mode-decomposition and multiplexing-detection scheme, and an OEM-water-filling policy, showing that our proposed OEM mmWave communications can significantly increase the SE as compared with the traditional massive-MIMO-based mmWave communications.

INDEX TERMS Millimeter-wave, massive multiple-input-multiple-output (MIMO), orbital angular momentum (OAM), OAM-embedded-MIMO (OEM), multiplicative spectrum-efficiency, parabolic antenna, mode-decomposition, multiplexing-detection, OEM-water-filling power allocation.

I. INTRODUCTION

The millimeter-wave (mmWave) communications with frequencies between 30 and 300 GHz has been treated as a powerful technique for the fifth-generation (5G) and 5G-beyond wireless communications networks [1]. Due to the high available bandwidth and small wavelength, the mmWave communications can potentially achieve high capacity as compared with the traditional radio wireless communications [2]. The massive-multiple-input-multiple-output (massive-MIMO) can be easily implemented in mmWave communications because the size of mmWave antenna can be made to be very small [3], [4].

However, although the mmWave communications can increase the capacity, it resorts to high bandwidth which cannot increase the spectrum-efficiency (SE) for wireless communications. In fact, as the traditional plane-electromagnetic (PE) wave based wireless communications are becoming more and more mature, it is now very hard to significantly increase the SE of traditional PE wave (which has linear momentum) based wireless

communications to meet the rapidly increasing of SE required by the extremely high-data traffics and tremendous amount of users [5]. The released International Mobile Telecommunications 2020 (IMT-2020) shows that the SE-gain for the 5G wireless networks is only 3-fold as compared with the fourth-generation (4G) wireless networks [6].

Fortunately, the electromagnetic wave not only has the characteristic of linear momentum which has been studied over a century, but also possesses the angular momentum which has attracted much attention during the past decade [7]–[12]. The orbital angular momentum (OAM), which is another important property of electromagnetic wave [7]–[9], has not been well studied yet. The electromagnetic wave carrying OAM has the helical phase fronts structure of the exponential function with the product of the OAM states/modes, azimuthal angle, and imaginary j. The OAM-based vortex wave has different topological charges, which are independent and orthogonal to each other, bridging a new way to significantly increase the SE of wireless communications using different OAM-modes [12]–[18].

Although the OAM-based vortex radio transmission can increase the SE of wireless communications, some academic researchers have shown that the communication over the orthogonal states of OAM is a subset of the solutions offered by multiple-input-multiple-output (MIMO) communications, thus offering no SE-gain as compared with the traditional multiplexing-MIMO communications [10], [11], [19]. However, noticing that the array-elements of one OAM-generation plate are fed with the same input signal [10], the OAM signal can be generated within one antenna which has several array-elements but only one RF-chain [20]. Thus, the OAM communications can be implemented within one array-elements-based antenna, where the distances among array-elements are not strictly required. On the other hand, in order to achieve the maximum SE for massive-MIMO communications, it is required that the distances among antennas in massive-MIMO system are larger than half of the carrier wavelength to achieve the optimal multiplexing of massive-MIMO communications. According to different displacement requirements for optimal OAM and massive-MIMO communications, it is clear that OAM and massive-MIMO cannot be entirely equally treated. Although now many research works regarding OAM transmission only consider the line-of-sight scenario, the OAM transmission can be used for multipath scenario when the phase change can be estimated. There exist some works considering the OAM transmission in multipath environment [21], [22]. Moreover, OAM and massive-MIMO are not conflicting with each other [23]. Thus, a question raised is that can we obtain the SE-gain of OAM while earning the SE-gain offered by the traditional multiplexing massive-MIMO communications?

In this paper, we solve the above-mentioned problem and give the answer YES. Some academic researchers have studied how to combine OAM and MIMO [23]–[25]. Oldoni *et al.* [23] proposed space-division demultiplexing in the OAM-based MIMO radio system and compared the capacities between the conventional MIMO system and OAM-based MIMO system. Zhang *et al.* [24] proposed plane spiral OAM-based MIMO system and compared with conventional MIMO. In addition, Murata *et al.* [25] proposed an analog eigenmode transmission technique based on the theory of OAM for short range communications. We build up the OAM embedded massive-MIMO (OEM) communication model, where the MIMO communications are performed among different uniform circular array (UCA) antennas and the OAM communications are performed among the array-elements corresponding to each UCA. Based on the OEM communication model, we design the parabolic antenna to converge the OAM signal. Then, we develop the mode-decomposition and multiplexing-detection scheme to obtain the signal corresponding to each OAM-mode of each transmit UCA antenna. We also develop the OEM-water-filling power allocation policy to obtain the maximum average multiplicative SE-gain for joint OAM and multiplexing massive-MIMO communications. We conduct extensive simulations to validate and evaluate our developed schemes, showing that our developed convergent OEM communications can significantly increase the average SE as compared with traditional multiplexing massive-MIMO communications.

The rest of this paper is organized as follows. Section II gives the OEM communication model. Section III designs the parabolic antenna to converge the OAM wave, proposes the mode-decomposition and multiplexing-detection scheme to obtain the signal on each OAM-mode of each transmit UCA antenna, develops the OEM-water-filling power allocation policy to maximize the average SE of OEM communications, and answers the question when the SE of OEM communication is larger than the SE of traditional massive-MIMO communication. Section IV evaluates our developed schemes and compares the SEs of OEM and traditional multiplexing massive-MIMO communications. The paper concludes with Section V.

II. OAM-EMBEDDED-MIMO COMMUNICATION MODEL

The OEM communication model is shown in Fig. 1, where N and M UCAs [26] are equidistantly around perimeter of the OEM transmit circle and the OEM receive circle, respectively. We denote by r_1 the radius of OEM transmit circle and OEM receive circle, r_2 the radius of UCAs [27], φ the included angle between the normal line of the OEM transmit circle and the line from the center of the OEM transmit circle to the center of the OEM receive circle, and θ the included angle between x-axis and the projection of the line from the center of the OEM transmit circle to the center of the OEM receive circle on the plane spanned by x-axis and y-axis. Each UCA at the transmitter is equipped with U array-elements, which are fed with the same input signal, but with a successive delay from array-element to array-element such that after a full turn the phase has been incremented by an integer multiple u of 2π with $1 \leq u \leq U$. Each UCA at the receiver is equipped with V array-elements with index from $v = 1$ to $v = V$. The OAM modes from $U/2$ to $U - 1$ are equivalent
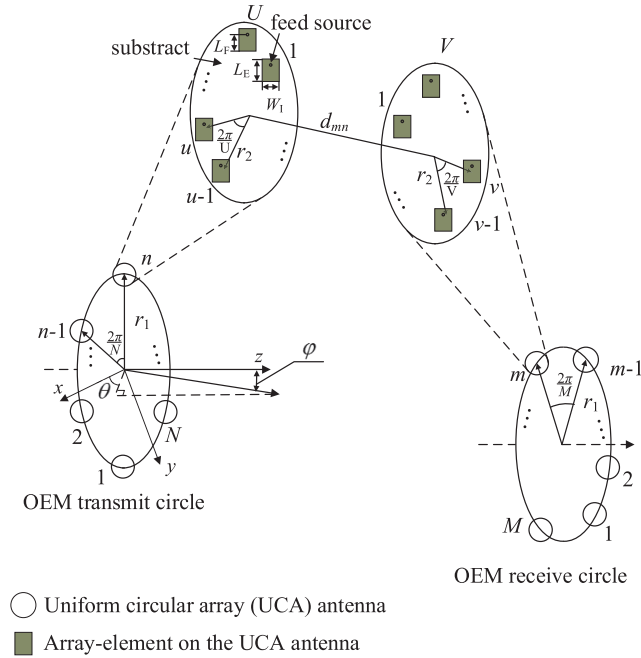
FIGURE 1. The OAM-embedded-MIMO communication model.

○ Uniform circular array (UCA) antenna

▪ Array-element on the UCA antenna

FIGURE 2. The geometry of each array-element.

to the OAM modes from $-U/2$ to -1. Thus, to easily write in the following equations, the OAM mode can be expressed as $0 \leq l \leq U - 1$. Each UCA at the transmitter is equipped with U array-elements with index from $u = 1$ to $u = U$. All array-elements within one transmit or receive UCA antenna share the same RF-chain. Thus, equipped with multiple array-elements, one transmit or receive UCA antenna is actually a single-antenna [20]. The N UCAs at the transmitter and the M UCAs at the receiver can be treated as N transmit and M receive antennas, forming a N-transmit-M-receive MIMO communication model. All UCAs are embedded in the MIMO, which is the OEM communication model. The OAM signal can be generated within one antenna which has several array-elements but only one RF-chain [20]. Thus, the OAM communications can be implemented within one array-elements-based antenna, where the distances among array-elements are not strictly required. Each UCA is one antenna in massive-MIMO system.

For each UCA antenna, we design the array and signal feeding to guarantee that the UCA antenna can generate OAM modes and form vortex waves to transmit signal. The geometry of each array-element is shown in Fig. 2, where W_I represents the width of array-elements, L_E denotes the length of array-elements, and L_F is the length of the feed source away from the bottom of array-element, respectively. The array-element, which is identified in yellow color, is put on the substrate which is identified in blue color. Each array-element is excited by coaxial feed method. All patch elements are fed by the signals with the same amplitude and different phases. The phase difference of adjacent array elements is $2\pi l/N$, where l is the index of OAM-mode. For simultaneous multiple OAM-modes transmission, the signals are linearly
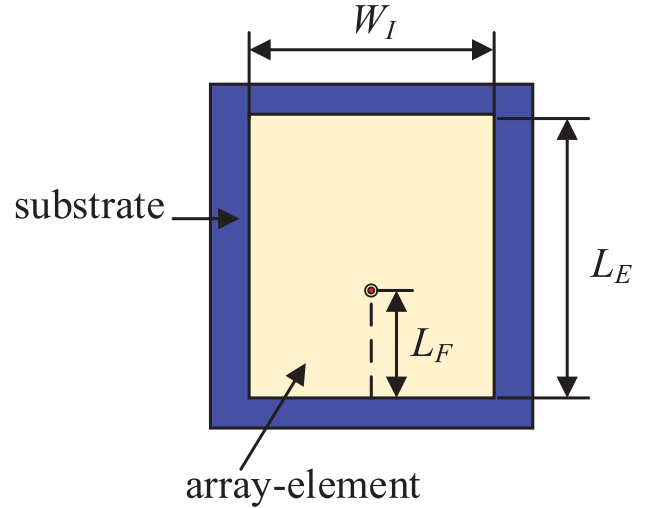
added and then feed to array-elements accordingly. In addition, U array-elements are equidistantly around the perimeter of each transmit UCA antenna. We set the distance between the centers of two adjacent array-elements as one carrier wavelength. We denote by W_I the width of array-elements, L_E the length of array-elements, and ε_r the relative permittivity of substrates, respectively. Then, we can calculate the width of array-elements as follows [28]–[30]:

$$W_I = \frac{\lambda}{2}\left(\frac{\varepsilon_r + 1}{2}\right)^{-\frac{1}{2}}. \quad (1)$$

where λ denotes the carrier wavelength. Then, we can calculate the effective permittivity, denoted by ε_e, for substrates as follows:

$$\varepsilon_e = \frac{\varepsilon_r + 1}{2} + \frac{\varepsilon_r - 1}{2}\left(1 + 12\frac{T_H}{W_I}\right)^{-\frac{1}{2}} \quad (2)$$

where T_H is the thickness of substrates and often be set as fixed value. Then, the length of wave guide, denoted by λ_e can be obtained from

$$\lambda_e = \frac{\lambda}{\sqrt{\varepsilon_e}} \quad (3)$$

and L_E can be derived as follows:

$$L_E = \frac{\lambda_e}{2} - 2\Delta L_E \quad (4)$$

where ΔL_E is the equivalent length of radiation gap and can be calculated as follows:

$$\Delta L_E = 0.412T_H\frac{(\varepsilon_e + 0.3)(W_I/T_H + 0.264)}{(\varepsilon_e - 0.258)(W_I/T_H + 0.8)}. \quad (5)$$

The feed source is located L_F long away from the bottom of each array-element and $W_I/2$ long away from left-side of the array-element. We denote by Z_w the wall admittance of array-element, which can be calculated as follows [28]:

$$Z_w = \frac{1}{0.00836\frac{W_I}{\lambda} + j0.01668\frac{\Delta L_E W_I \varepsilon_e}{T_H \lambda}}. \quad (6)$$

We denote by Z_0 the characteristic impedance of each array-element. Then, the input admittance at the feed source, denoted by Y_1, can be obtained as follows:

$$Y_1 = \frac{1}{Z_0} \left(\frac{Z_0 \cos \psi L_F + jZ_w \sin \psi L_F}{Z_w \cos \psi L_F + jZ_0 \sin \psi L_F} \right.$$
$$\left. + \frac{Z_0 \cos \psi (L_E - L_F) + jZ_w \sin \psi (L_E - L_F)}{Z_w \cos \psi (L_E - L_F) + jZ_0 \sin \psi (L_E - L_F)} \right) \quad (7)$$

where ψ is a constant representing the phase of medium. Then, the input impedance, denoted by Z_{in}, for each array-element can be obtained as follows:

$$Z_{in} = \frac{1}{Y_1} + j \frac{377}{\sqrt{\varepsilon_r}} \tan \left(\frac{2\pi T_H}{\lambda} \right). \quad (8)$$

As a result, when the input impedance for each array-element is equal to 50 Ω, we can obtain L_F as follows:

$$L_F = \frac{L_E}{2} \left(1 - \frac{1}{\sqrt{\xi_{re}}} \right) \quad (9)$$

where

$$\xi_{re} = \frac{\varepsilon_r + 1}{2} + \frac{\varepsilon_r - 1}{2} \left(1 + 12 \frac{T_H}{L_E} \right)^{-\frac{1}{2}}. \quad (10)$$

III. ACHIEVING MAXIMUM MULTIPLICATIVE SPECTRUM EFFICIENCY FOR OEM COMMUNICATIONS

In the section, we mainly propose the mode-decomposition and multiplexing-detection scheme as well as the optimal power allocation policy to maximize the multiplicative SE for convergent OEM communications. First, we design the parabolic antenna based converging method for OAM wave to enable the efficient high-order OAM-mode. Second, we propose the mode-decomposition and multiplexing-detection scheme to resolve the transmit signal on each OAM-mode of each transmit antenna. Third, we develop the OEM-waterfilling power allocation policy to maximize the multiplicative SE for OEM communications. At last, we answer the question when we need to use the OEM communications.

A. PARABOLIC ANTENNA BASED OAM WAVE CONVERGING

Since one UCA consisting of U array-elements can generate U OAM modes, according to the principle of OAM communications [10], [31], [32], we give the signal at the uth ($1 \leq u \leq U$) array-element on the nth ($1 \leq n \leq N$) transmit UCA antenna for the total U OAM modes, denoted by $x_{n,u}$, as follows:

$$x_{n,u} = \sum_{l=0}^{U-1} \frac{1}{\sqrt{U}} s_{n,l} e^{j\phi_u l} = \sum_{l=0}^{U-1} \frac{1}{\sqrt{U}} s_{n,l} e^{j\frac{2\pi(u-1)}{U}l} \quad (11)$$

where $0 \leq l \leq U - 1$ is the OAM-mode number, ϕ_u is the azimuthal angle (defined as the angular position on a plane perpendicular to the axis of propagation) corresponding to the uth array-element, and $s_{n,l}$ is the signal on the lth OAM-mode of the nth transmit UCA antenna. The emitted signal, denoted by $\tilde{x}_{n,l}$, of the lth mode from the nth transmit UCA antenna

can be treated as a continuous signal and can be expressed as follows:

$$\tilde{x}_{n,l} = s_{n,l} e^{j\phi l} \quad (12)$$

where $0 \leq \phi < 2\pi$ is the continuous phase parameter.

For the nth transmit UCA antenna and the mth receive UCA antenna, we can derive the received signal, denoted by $r_{mn,v,l}$, for the lth OAM-mode on the vth receive array-element as follows:

$$r_{mn,v,l} = \sum_{u=1}^{U} h_{mn,vu} \tilde{x}_{n,l} \quad (13)$$

where $h_{mn,vu}$ denotes the channel amplitude gain corresponding to the lth OAM-mode from the uth transmit array-element to the vth receive array-element. The expression for $h_{mn,vu}$ is given as follows:

$$h_{mn,vu} = \frac{\beta \lambda e^{-j\frac{2\pi}{\lambda}|\vec{d}_{mn} - \vec{r}_u + \vec{g}_v|}}{4\pi \sqrt{U} |\vec{d}_{mn} - \vec{r}_u + \vec{g}_v|} \quad (14)$$

where β denotes all relevant constants such as attenuation and phase rotation caused by antennas and their patterns on both sides, $\vec{r}_u$ and $\vec{g}_v$ are the vectors from the center of transmit UCA antenna to the uth transmit array-element and from the center of receive UCA antenna to the vth receive array-element, respectively, where $\vec{d}_{mn}$ is the vector from the center of the mth transmit UCA antenna and the center of the nth receive UCA antenna, $|\vec{d}_{mn} - \vec{r}_u + \vec{g}_v|$ represents the distance between the uth transmit array-element on the nth transmit UCA antenna and the vth receive array-element on the mth receive UCA antenna. Because of $|\vec{d}_{mn}| \gg |\vec{r}_u|$ and $|\vec{d}_{mn}| \gg |\vec{g}_v|$, we approximate $|\vec{d}_{mn} - \vec{r}_u + \vec{g}_v|$ at the denominator of Eq. (14) to $|\vec{d}_{mn}|$ and $|\vec{d}_{mn} - \vec{r}_u + \vec{g}_v|$ at the nominator of Eq. (14) to $|\vec{d}_{mn}| - \vec{d}_{mn}\vec{r}_u / |\vec{d}_{mn}|$. We denote by $d_{mn} = |\vec{d}_{mn}|$. Thus, we can rewrite $h_{mn,vu}$ as follows:

$$h_{mn,vu} \approx \frac{\beta \lambda}{4\pi \sqrt{U} d_{mn}} \exp \left[-j\frac{2\pi}{\lambda} \left(d_{mn} - \frac{\vec{d}_{mn}\vec{r}_u}{d_{mn}} \right) \right]. \quad (15)$$

Based on Eqs. (13) and (15), we can derive the equivalent channel amplitude gain, denoted by $h_{mn,vu,l}$, for the lth OAM-mode corresponding to the uth transmit array-element and the vth receive array-element as follows:

$$h_{mn,vu,l} = \sum_{u=1}^{U} \frac{1}{h_{mn,vu}} e^{j\frac{2\pi(u-1)}{U}l}$$
$$\approx \frac{\beta \lambda}{4\pi} \sum_{u=1}^{U} \frac{1}{\sqrt{U}} e^{j\frac{2\pi(u-1)}{U}l} \frac{e^{-j\frac{2\pi}{\lambda}d_{mn}} e^{j\frac{2\pi \vec{d}_{mn}\vec{r}_u}{\lambda d_{mn}}}}{d_{mn}} \quad (16)$$

where

$$\vec{d}_{mn} = (d_{mn} \sin(\varphi) \cos(\theta), d_{mn} \sin(\varphi) \sin(\theta), d_{mn} \cos(\varphi)) \quad (17)$$

and

$$\vec{r}_u = \left(r_2 \cos\left(\frac{2\pi(u-1)}{U} \right), r_2 \sin\left(\frac{2\pi(u-1)}{U} \right) \right). \quad (18)$$

Thus, $h_{mn,vu,l}$ can be obtained as follows:

$$h_{mn,vu,l} = \frac{\beta\lambda e^{-j\frac{2\pi}{\lambda}d_{mn}}}{4\pi\sqrt{U}d_{mn}}$$
$$\times \sum_{u=1}^{U} e^{j\frac{2\pi(u-1)}{U}l} e^{j\frac{2\pi}{\lambda}r_2 \cos\left[\frac{2\pi(u-1)}{U} - \theta \right]\sin\varphi}. \quad (19)$$

When U is relatively large enough, we denote by $\theta' = 2\pi(u-1)/U - \theta$ and we have

$$\frac{e^{-j\theta l}j^l}{U} \sum_{u=1}^{U} e^{j\frac{2\pi(u-1)}{U}l} e^{j\frac{2\pi}{\lambda}r_2 \cos\left[\frac{2\pi(u-1)}{U} - \theta \right]\sin\varphi}$$
$$\approx \frac{j^l}{2\pi} \int_0^{2\pi} e^{j\theta' l} e^{j\frac{2\pi}{\lambda}r_2 \sin\varphi \cos\theta'} d\theta'$$
$$= J_l\left(\frac{2\pi}{\lambda}r_2 \sin\varphi \right) \quad (20)$$

where

$$J_l(\alpha) = \frac{j^l}{2\pi} \int_0^{2\pi} e^{jl\tau} e^{j\alpha \cos\tau} d\tau \quad (21)$$

is the l-order Bessel function [33]. Then, based on Eq. (20), we can rewrite $h_{mn,vu,l}$ as follows:

$$h_{mn,vu,l} \approx \frac{\beta\lambda e^{-j\frac{2\pi}{\lambda}d_{mn}}\sqrt{U}e^{j\theta l}j^{-l}}{4\pi d_{mn}} J_l\left(\frac{2\pi}{\lambda}r_2 \sin\varphi \right). \quad (22)$$

Equation (22) shows that the channel amplitude gains corresponding to the lth OAM-mode from the uth array-element on the nth transmit UCA antenna to the vth array-element on the mth receive UCA antenna are the same for $1 \le u \le U$ and $1 \le v \le V$. Thus, the UCA based OAM signal can be treated as sending from the center of the transmit UCA antenna and receiving at the center of the receive UCA antenna. Then, we have the channel amplitude gain, denoted by $h'_{mn,l}$, for the lth mode corresponding to the nth transmit UCA antenna and the mth receive UCA antenna as follows:

$$h'_{mn,l} = \frac{\beta\lambda e^{-j\frac{2\pi}{\lambda}d_{mn}}\sqrt{U}e^{j\theta l}j^{-l}}{4\pi d_{mn}} J_l\left(\frac{2\pi}{\lambda}r_2 \sin\varphi \right). \quad (23)$$

Observing Eq. (23), we can find that the transmit UCA antenna causes the OAM signal like going through the Bessel-form channel. According to the characteristics of Bessel function, $h'_{mn,l}$ severely decreases as l increases, resulting in very small received SNR when using the high order (The OAM-mode number is relatively large) OAM communications. That is not what we expected since we aim to obtain the maximum SE combined from all orthogonal OAM-modes. In fact, it has been shown that the electromagnetic wave with OAM is centrally hollow and divergent [34]. Also, as the OAM-mode number increases, the corresponding electromagnetic wave becomes even more divergent. Therefore,
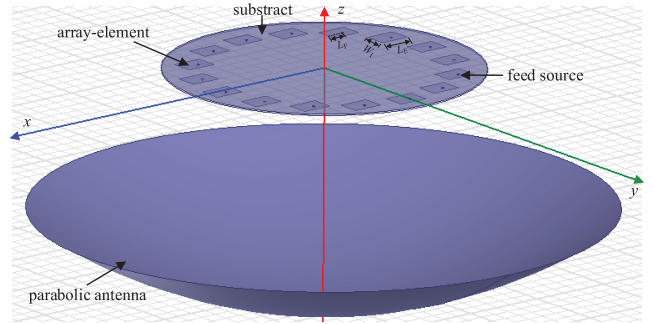

FIGURE 3. The designed parabolic antenna for converging OAM waves.

if the OAM-mode number is relatively large, it is impossible to get high SE for the OAM communications since the received SNR corresponding to the large OAM-mode number is very small as compared with the PE wave based communications.

To significantly increase the received SNR for each mode of OAM communications, the electromagnetic waves corresponding to all OAM-modes need to be convergent. Generally, the electromagnetic waves can be converged using the backscatter of parabolic antenna, the refraction of lens antenna, and the diffraction-free super-surface material [35], etc. These schemes can be treated as making a pre-distortion before transmission. Here, we propose the parabolic antenna based converging method to get high SE for high order OAM (l is relatively large) communications. Each UCA needs to equip one parabolic antenna to converge the OAM signal. The center of UCA is placed at the focus of the parabolic antenna with array-elements facing the parabolic antenna. One example for joint UCA and parabolic antenna model is shown in Fig. 3, which is a profile for joint transmit UCA antenna and parabolic antenna model designed in HFSS.

To design the parabolic antenna [36], [37], we denote by F and D the focal length and the diameter of aperture, respectively. Given the gain, denoted by G, of parabolic antenna and the efficiency of aperture's utilization, denoted by η, we can derive the diameter of aperture as follows:

$$D = \frac{\lambda\sqrt{G\eta}}{\pi}. \quad (24)$$

Then, we can obtain the focal length as follows:

$$F = \kappa D \quad (25)$$

where κ is the focal length to aperture diameter ratio of parabolic antenna. The value of κ is often chosen between 0.25 and 0.5. Then, the equation for parabolic antenna can be derived as follows:

$$Z = (X^2 + Y^2)/4F \quad (26)$$

where X, Y, and Z are the x-axis, y-axis, and z-axis coordinates for the parabolic antenna.

After converging by the parabolic antenna, the impact of item $J_l(2\pi r_2 \sin\varphi/\lambda)$ can be greatly reduced. Then,

the equivalent channel amplitude gain, denoted by $\widetilde{h}_{mn,l}$, for the lth mode corresponding to the nth transmit UCA antenna and the mth receive UCA antenna can be modeled as follows:

$$\widetilde{h}_{mn,l} = A_l h'_{mn,l} \tag{27}$$

where A_l denotes the amplitude gain on the lth OAM-mode caused by the backscatter of parabolic antenna. We assume that the parabolic antenna can reduce the item $J_l(2\pi r_2 \sin \varphi/\lambda)$ to δ_0, where δ_0 is a constant very close to 1[26]. Thus, we have $A_l = 1/J_l(2\pi r_2 \sin \varphi/\lambda)$.

B. MODE-DECOMPOSITION AND MULTIPLEXING-DETECTION SCHEME

At the receiver, the convergent vortex signal received at the mth receive UCA antenna, denoted by $r_{m,v}$, can be obtained as follows:

$$r_{m,v} = \sum_{l=0}^{U-1} \sum_{n=1}^{N} \widetilde{h}_{mn,l} s_{n,l}. \tag{28}$$

The convergent vortex signal can be spatially sampled at each array-element of the receive UCA antenna. Then, after the sampling, the signal received at the vth array-element of the mth receive UCA antenna, denoted by $y_{m,v}$, can be derived as follows:

$$y_{m,v} = \sum_{l=0}^{U-1} \sum_{n=1}^{N} A_l \sum_{u=1}^{U} \frac{1}{\sqrt{U}} h_{mn,uv} s_{n,l} e^{j\frac{2\pi(v-1)}{V} l} + w_{m,v} \tag{29}$$

where $w_{m,v}$ denotes the received noise at the vth array-element of the mth receive UCA antenna. To obtain the received signal on the l_0th $(0 \le l_0 \le U-1)$ mode sent from all transmit UCA antennas, we multiply $y_{m,v}$ with $\exp\{-j[2\pi(v-1)l_0]/V\}$ and we have the received signal, denoted by y_{m,v,l_0}, on the l_0 mode corresponding to the vth array-element of the mth receive UCA antenna as follows:

$$\begin{aligned}
y_{m,v,l_0} &= y_{m,v} e^{-j\frac{2\pi(v-1)}{V} l_0} \\
&= \sum_{n=1}^{N} \sum_{l=0,l\neq l_0}^{U-1} A_l \sum_{u=1}^{U} \frac{1}{\sqrt{U}} h_{mn,uv} s_{n,l} e^{j\frac{2\pi(v-1)}{V}(l-l_0)} \\
&\quad + \sum_{n=1}^{N} A_l \sum_{u=1}^{U} \frac{1}{\sqrt{U}} h_{mn,uv} s_{n,l_0} + w_{m,v} e^{-j\frac{2\pi(v-1)}{V} l_0}.
\end{aligned} \tag{30}$$

Observing Eq. (15), we can find that $h_{mn,uv}$ is independent of v. Thus, the polynomials $\frac{1}{\sqrt{U}} h_{mn,uv} s_{n,l}$ corresponding to different v are the same for different $e^{j\frac{2\pi(v-1)}{V}(l-l_0)}$ in Eq. (30). Then, the received signal, denoted by $\widetilde{y}_{m,l_0}$, on the l_0th mode of the mth receive UCA antenna can be derived as follows:

$$\begin{aligned}
\widetilde{y}_{m,l_0} &= \sum_{v=1}^{V} y_{m,v,l_0} \\
&= \sum_{v=1}^{V} \sum_{n=1}^{N} A_l \sum_{u=1}^{U} \frac{1}{\sqrt{U}} h_{mn,uv} s_{n,l_0} + \widetilde{w}_{m,l_o}
\end{aligned} \tag{31}$$

where $\widetilde{w}_{m,l_0}$ denotes the received noise on the l_0th mode corresponding to the mth receive UCA antenna. Now, we have obtained the estimated decomposed signal, specified in Eq. (31), for all OAM-modes $(0 \le l_0 \le U-1)$. It is clear that $\widetilde{y}_{m,l_0}$ follows the standard form of received signal as that in multiplexing-MIMO communications.

We denote by $y_l = [\widetilde{y}_{1,l}, \widetilde{y}_{2,l}, \cdots, \widetilde{y}_{M,l}]^T$ and $w_l = [\widetilde{w}_{1,l}, \widetilde{w}_{2,l}, \cdots, \widetilde{w}_{M,l}]^T$ the received signal and noise, respectively, corresponding to the lth mode, where $(\cdot)^T$ represents the transpose operation. Using the zero-forcing detection scheme, the estimate value of transmit signal, denoted by $\widehat{s}_l$, can be derived as follows:

$$\begin{aligned}
\widehat{s}_l &= (H_l^H H_l)^{-1} H_l^H y_l \\
&= s_l + (H_l^H H_l)^{-1} H_l^H w_l
\end{aligned} \tag{32}$$

where $(\cdot)^H$ denotes the conjugation operation, w_l is the received noise on the lth mode, and

$$H_l = V \begin{bmatrix} \widetilde{h}_{11,l} & \widetilde{h}_{12,l} & \cdots & \widetilde{h}_{1N,l} \\ \widetilde{h}_{21,l} & \widetilde{h}_{22,l} & \cdots & \widetilde{h}_{2N,l} \\ \vdots & \vdots & \ddots & \vdots \\ \widetilde{h}_{M1,l} & \widetilde{h}_{M2,l} & \cdots & \widetilde{h}_{MN,l} \end{bmatrix} \tag{33}$$

is the amplitude gain matrix of all channels on the lth mode. Then, the received channel signal-to-noise-ratio (SNR), denoted by SNR_l, for the lth model can be derived as follows:

$$SNR_l = \frac{|s_l|^2}{\sigma_l^2 |(H_l^H H_l)^{-1} H_l^H|^2} \tag{34}$$

where σ_l^2 denotes the variance of received noise corresponding to the lth mode.

C. OEM-WATER-FILLING POWER ALLOCATION POLICY

For the OEM communications, the instantaneous SE, denoted by C_{OEM}, can be derived as follows:

$$\begin{aligned}
C_{OEM} &= \sum_{l=0}^{U-1} \log_2 \det \left(I + \frac{|s_l|^2}{\sigma_l^2 |(H_l^H H_l)^{-1} H_l^H|^2} \right) \\
&= \sum_{l=0}^{U-1} \sum_{i=1}^{rank(H_l)} \log_2 \left(1 + P_{i,l} \gamma_{i,l} \right)
\end{aligned} \tag{35}$$

where I is the identity matrix, $\gamma_{i,l} = \overline{P}/[\sigma_l^2 |(H_l^H H_l)^{-1} H_l^H|^2]$ represents the received SNR corresponding to matrix H_l with $\overline{P}$ representing the upper-bound of total power, $rank(H_l)$ denotes the rank of H_l, and $P_{i,l}$ denotes the power allocation policy. We aim to maximize the SE for OEM communications. Thus, we formulate the average SE maximization problem, denoted by $P1$, as follows:

$$P1 : \max \mathbb{E}_{\gamma} \left[\sum_{l=0}^{U-1} \sum_{i=1}^{rank(H_l)} \log_2 \left(1 + P_{i,l} \gamma_{i,l} \right) \right] \tag{36}$$

$$\text{s.t. : } 1). \ \mathbb{E}_{\gamma} \left[\sum_{l=0}^{U-1} \sum_{i=1}^{rank(H_l)} P_{i,l} \right] \le \overline{P}; \tag{37}$$

2). $P_{i,l} \geq 0, \forall l \in [0, U-1], \forall i \in [1, rank(\boldsymbol{H}_l)]$, (38)

where

$$\boldsymbol{\gamma} = \begin{bmatrix} \gamma_{1,0} & \gamma_{1,1} & \cdots & \gamma_{1,U-1} \\ \gamma_{2,0} & \gamma_{2,1} & \cdots & \gamma_{2,U-1} \\ \vdots & \vdots & \ddots & \vdots \\ \gamma_{rank(\boldsymbol{H}_l),0} & \gamma_{rank(\boldsymbol{H}_l),1} & \cdots & \gamma_{rank(\boldsymbol{H}_l),U-1} \end{bmatrix} \quad (39)$$

is the instantaneous received SNR for all channels of the OEM communications and $\mathbb{E}_{\boldsymbol{\gamma}}\{\cdot\}$ is the expectation operation with respect to $\boldsymbol{\gamma}$. We assume that the channels corresponding to all modes of all UCAs follow the Rayleigh distribution, where the probability density function (PDF), denoted by $p(\gamma_{i,l})$, is given by $p(\gamma_{i,l}) = \exp(-\gamma_{i,l}/\overline{\gamma}_{i,l})/\overline{\gamma}_{i,l}$ and $\overline{\gamma}_{i,l}$ denotes the average received SNR.

It is clear that **P1** is a strictly convex optimization problem [38]. To solve **P1**, we construct the Lagrangian function for **P1**, denoted by J, as follows:

$$J = \mathbb{E}_{\boldsymbol{\gamma}}\left[\sum_{l=0}^{U-1}\sum_{i=1}^{rank(\boldsymbol{H}_l)} \log_2\left(1 + P_{i,l}\gamma_{i,l}\right)\right] + \sum_{i=1}^{rank(\boldsymbol{H}_l)}\sum_{l=0}^{U-1} \epsilon_{i,l}P_{i,l}$$
$$- \mu\left(\mathbb{E}_{\boldsymbol{\gamma}}\left[\sum_{l=0}^{U-1}\sum_{i=1}^{rank(\boldsymbol{H}_l)} P_{i,l}\right] - \overline{P}\right) \quad (40)$$

where $\mu \geq 0$ and $\epsilon_{i,l} \geq 0$ ($1 \leq i \leq rank(\boldsymbol{H}_l), 0 \leq l \leq U-1$) are the Lagrangian multipliers associated with the constraints specified by Eqs. (37) and (38), respectively. Taking the derivative for J with the respect to $P_{i,l}$ and setting the derivative equal to zero, we can obtain a set of $\sum_{l=0}^{U-1} rank(\boldsymbol{H}_l)$ equations as follows:

$$\frac{\partial J}{\partial P_{i,l}} = \frac{\frac{1}{\log 2}}{1 + P_{i,l}\gamma_{i,l}}\gamma_{i,l}p_{\Gamma}(\gamma) - \mu p_{\Gamma}(\gamma) + \epsilon_{i,l} = 0 \quad (41)$$

where $p_{\Gamma}(\gamma)$ is the probability density function corresponding to the channel. According to the principle of complementary slackness, we have $\epsilon_{i,l}P_{i,l} = 0$ for $\forall l \in [0, U-1]$ and $\forall i \in [1, rank(\boldsymbol{H}_l)]$. Correspondingly, we consider two different cases as follows:

Case A: The inequality $P_{i,l} > 0$ holds for $\forall l \in [0, U-1]$ and $\forall i \in [1, rank(\boldsymbol{H}_l)]$. Under this case, all channels corresponding to all OAM-modes of all transmit UCA antennas are assigned non-zero power for data transmission. Thus, based on the complementary slackness, we have $\epsilon_{i,l} = 0$ for $\forall l \in [0, U-1]$ and $\forall i \in [1, rank(\boldsymbol{H}_l)]$. Then, Eq. (41) can be reduced to

$$\frac{\frac{\gamma_{i,l}}{\log 2}}{1 + P_{i,l}\gamma_{i,l}} - \mu^* = 0. \quad (42)$$

where μ^* is the optimal Lagrangian multiplier corresponding to μ. Solving Eq. (42), we can obtain the optimal power allocation policy for **Case A** as follows:

$$P_{i,l} = \frac{1}{\mu^* \log 2} - \frac{1}{\gamma_{i,l}},$$
$$\text{for } 1 \leq i \leq rank(\boldsymbol{H}_l) \text{ and } 0 \leq l \leq U-1, \quad (43)$$

where the optimal value for μ^* can be numerically obtained by substituting $P_{i,l}$ into

$$\mathbb{E}_{\boldsymbol{\gamma}}\left[\sum_{l=0}^{U-1}\sum_{i=1}^{rank(\boldsymbol{H}_l)} P_{i,l}\right] = \overline{P}. \quad (44)$$

We define

$$\mathcal{N}_1 = \{(i, l)|1 \leq i \leq rank(\boldsymbol{H}_l), 0 \leq l \leq U-1\} \quad (45)$$

and we also define $\mathcal{N}_2$ as the index-set which satisfies the strict inequality as follows:

$$\mathcal{N}_2 \triangleq \left\{(i, l) \in \mathcal{N}_1 \left| \frac{1}{\mu^* \log 2} - \frac{1}{\gamma_{i,l}} > 0\right.\right\}. \quad (46)$$

Then, Eq. (43) is the optimal solution only if $\mathcal{N}_2 = \mathcal{N}_1$. Otherwise, if $\mathcal{N}_2 \subset \mathcal{N}_1$, we need to consider the following case.

Case B: There exist some $P_{i,l}$ such that $P_{i,l} = 0$. If $\mathcal{N}_2 \subset \mathcal{N}_1$, there certainly exist some $P_{i,l}$ such that $P_{i,l} = 0$. That means some OAM-modes (maybe some transmit UCAs) are not assigned power and are not used for data transmission. We give the following lemma.

Lemma 1: If $(i, l) \notin \mathcal{N}_2$, then $P_{i,l} = 0$.

Proof: We need to show that for any non-empty subset $\mathcal{C} \subseteq \overline{\mathcal{N}_2}$, there is no power allocation policy $P_{i,l}$ such that $P_{i,l} > 0$ for all $(i, l) \in (\mathcal{C} \cup \mathcal{N}_2)$.

If $\mathcal{C} = \overline{\mathcal{N}_2}$, we have already known that there is no power allocation policy.

Otherwise, if $\mathcal{C} \subset \overline{\mathcal{N}_2}$, we suppose that there exists such a power allocation policy so that it can be expressed as

$$P_{i,l} = \begin{cases} \frac{1}{\mu^* \log 2} - \frac{1}{\gamma_{i,l}}, & (i, l) \in (\mathcal{C} \cup \mathcal{N}_2); \\ 0, & \text{otherwise.} \end{cases} \quad (47)$$

According to Eq. (47), we can select an element $(i', l') \in \mathcal{C}$, which satisfies $P_{i',l'} > 0$. Thus, we can obtain

$$\gamma_{i',l'} > \mu^* \log 2. \quad (48)$$

On the other hand, according the definition of $\mathcal{N}_2$ specified in Eq. (46) and $\overline{\mathcal{N}_2}$, we know

$$\gamma_{i',l'} < \mu^* \log 2 \quad (49)$$

which is opposed to Eq. (48). Therefore, such a power allocation policy does not exist and Lemma 1 follows. ∎

Following the same procedure as that used in **Case A**, if the strict inequality $P_{i,l} > 0$ holds for all $(i, l) \in \mathcal{N}_2$, we can obtain the optimal power allocation policy as follows:

$$P_{i,l} = \begin{cases} \frac{1}{\mu^* \log 2} - \frac{1}{\gamma_{i,l}}, & (i, l) \in \mathcal{N}_2; \\ 0, & \text{otherwise.} \end{cases} \quad (50)$$

Otherwise, if not all $(i, l) \in \mathcal{N}_2$ satisfy the strict inequality $P_{i,l} > 0$, we need to further divide $\mathcal{N}_2$ and repeat the procedure again. In summary, the optimal power allocation policy, called the OEM-water-filling power allocation policy, is given by Algorithm 1 in the following.

Algorithm 1 The OEM-Water-Filling Power Allocation Policy

1) **Initialization**
   a) Obtain $\mathcal{N}_2$ by Eq. (46)
   b) $k = 2$
2) **While** ($\mathcal{N}_k \neq \mathcal{N}_{k-1}$)
   a) $\mathcal{N}_{k+1} = \left\{ (i, l) \in \mathcal{N}_k \middle| \frac{1}{\mu^* \log 2} - \frac{1}{\gamma_{i,l}} > 0 \right\}$
   b) $k = k + 1$
3) **Obtain the optimal power allocation policy**
   a) Denote $\mathcal{N}^* = \mathcal{N}_k$
   b)
$$lP_{i,l} = \begin{cases} \frac{1}{\mu^* \log 2} - \frac{1}{\gamma_{i,l}}, & (i, l) \in \mathcal{N}^*; \\ 0, & \text{otherwise.} \end{cases}$$
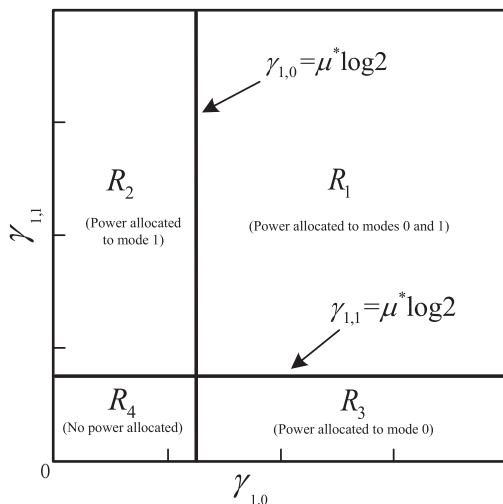
FIGURE 4. The regions for the OEM-water-filling power allocation policy corresponding to the two OAM-modes case ($l = 0$ and $l = 1$).

To show the execution procedure of our developed OEM-water-filling power allocation policy, we demonstrate a particular case when $i = 1$ and $l \in \{0, 1\}$ for OEM communications. Using Algorithm 1, we can see that the optimal power allocation policy partitions the SNR-plane $(\gamma_{1,0}, \gamma_{1,1})$ into four exclusive regions by the lines as shown in Fig. 4. If $(\gamma_{1,0}, \gamma_{1,1})$ falls into region R_1, both two subchannels corresponding to $l = 0$ and $l = 1$ will be assigned with power for data transmission. The boundaries of region R_1 are determined by $\gamma_{1,0} = \mu^* \log 2$ and $\gamma_{1,1} = \mu^* \log 2$ which are obtained by solving the boundary condition $\mathcal{N}_2 = \mathcal{N}_1$. On the other hand, if $(\gamma_{1,0}, \gamma_{1,1})$ falls into either R_2 or R_3, then only one of the subchannels will be assigned with power. Otherwise, if $(\gamma_{1,0}, \gamma_{1,1})$ belongs to region R_4, there is no power allocated to any subchannel and the system will be in an outage state.

Substituting the OEM-water-filling power allocation policy into Eq. (35), we can obtain the maximum average SE,

denoted by C^*_{OEM}, for OEM communications as follows:

$$C^*_{OEM} = \mathbb{E}_{\boldsymbol{\gamma}} \left[\sum_{l=0}^{U-1} \sum_{i=1}^{rank(\boldsymbol{H}_l)} \log_2 \left(\frac{\gamma_{i,l}}{\mu^* \log 2} \right) \right]. \quad (51)$$

To compare the SE of OEM communications with that of the traditional multiplexing-MIMO communications, we also give the maximum average SE, denoted by C^*_{MIMO}, for the traditional multiplexing-MIMO communications as follows:

$$C^*_{MIMO} = \sum_{i=1}^{rank(\widetilde{\boldsymbol{H}})} \log_2 \left(1 + \widetilde{P}_i \widetilde{\gamma}_i \right) \quad (52)$$

where $rank(\widetilde{\boldsymbol{H}})$ denotes rank corresponding to the MIMO communication channel matrix $\widetilde{\boldsymbol{H}}$, $\widetilde{P}_i$ is the optimal power allocation [39] for MIMO communications and $\widetilde{\gamma}_i$ is the received SNR corresponding to matrix $\widetilde{\boldsymbol{H}}$.

For OEM communication, each UCA consists of U array-elements at the transmitter and V array-elements at the receiver, respectively. However, all array-elements within one transmit or receive UCA antenna share the same RF-chain. Thus, each UCA antenna is actually a single-antenna. Based on Eqs. (51) and (52), we can calculate the average SEs of OEM and traditional massive-MIMO communications under the same number of transmit and receive antennas.

When the distance between neighboring antennas in UCA is less than $\lambda/2$ for massive-MIMO communications, mutual coupling between the two neighboring antennas arises, thus resulting in the decrease of SE for massive-MIMO system. However, when the distance between neighboring array-elements in UCA is less than $\lambda/2$ for OEM communications, the SE still can be calculated by Eq. (51). Thus, OEM can be used when the distance between neighboring antennas in UCA is less than $\lambda/2$.

D. WHEN DO WE USE THE OEM COMMUNICATIONS?

The traditional multiplexing-MIMO requires that the distance between two adjacent antennas needs to be not less than half of the carrier wavelength [40], [41], which limits the displacement of multiple antennas in MIMO systems. However, there is no minimum distance restriction on OAM vortex communications, thus bridging the new way to achieve very high SE.

As for our proposed OEM model, if the distance between two adjacent UCA array-elements is less than half of the carrier wavelength, the UCA-based OAM vortex communications can be embedded into the massive-MIMO system, forming the OEM communication to achieve larger SE than the traditional massive-MIMO system.

We denote by $d_a(r_1, N)$ and $d_e(r_2, U)$ the distances between the centers of two adjacent UCAs and between the center of two adjacent array-elements, respectively. Then, we have

$$\begin{cases} d_a(r_1, N) = 2r_1 \sin(\frac{\pi}{N}) \\ d_e(r_2, U) = 2r_2 \sin(\frac{\pi}{U}). \end{cases} \quad (53)$$
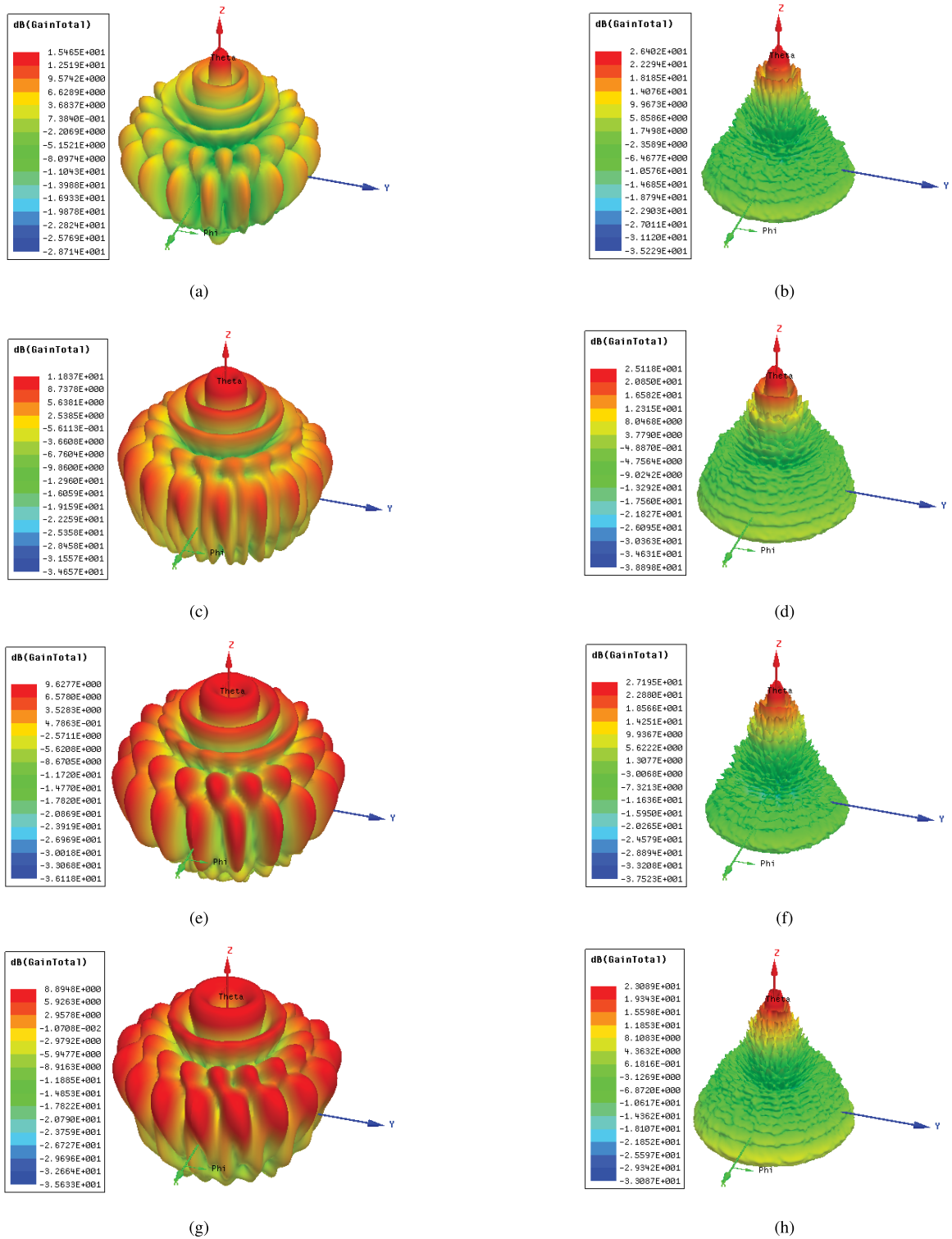
FIGURE 5. The directional diagram for non-convergent and convergent OEM waves with $N = 1$ and $M = 1$. (a) Mode 0 (Non-convergent OEM, $l = 0$). (b) Mode 0 (Convergent OEM, $l = 0$). (c) Mode 1 (Non-convergent OEM, $l = 1$). (d) Mode 1 (Convergent OEM, $l = 1$). (e) Mode 2 (Non-convergent OEM, $l = 2$). (f) Mode 2 (Convergent OEM, $l = 2$). (g) Mode 3 (Non-convergent OEM, $l = 3$). (h) Mode 3 (Convergent OEM, $l = 3$).

Based on Eq. (53), we can analyze two scenarios as follows:

Scenario I: $d_a(r_1, N) > \lambda/2$ and $d_e(r_2, U) \leq \lambda/2$. Under this scenario, the OAM signal can be generated by every UCA
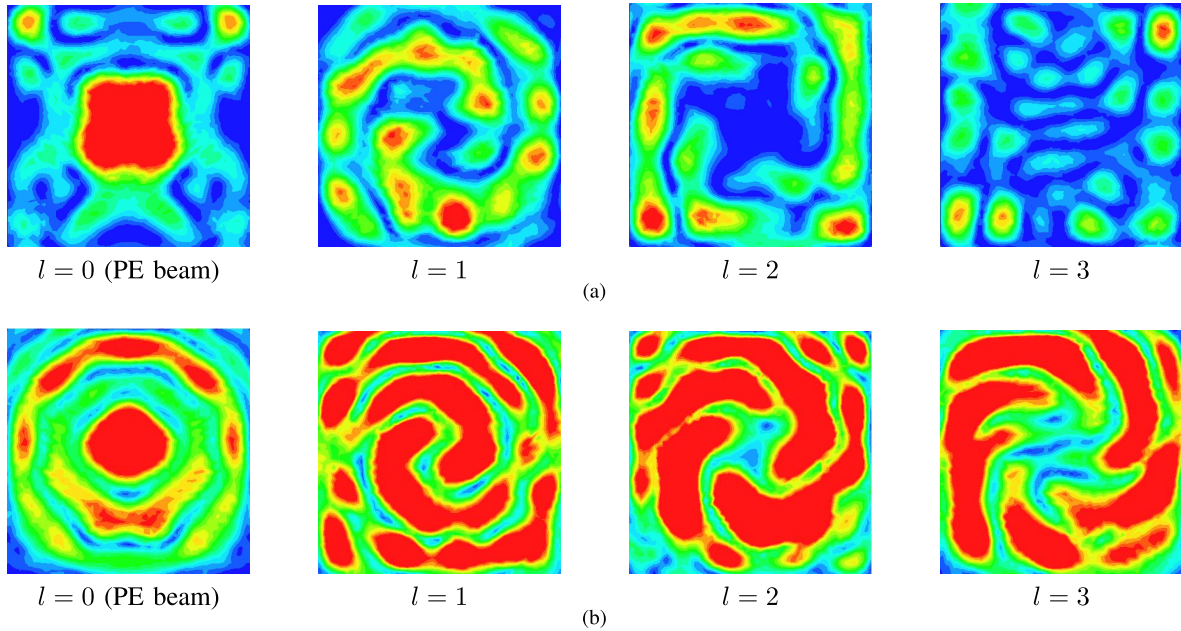
FIGURE 6. The E field of unconverged and converged OAM beams observed from the vertical direction. (a) The E field of unconverged OAM beams (vertical direction). (b) The E field of converged OAM beams (vertical direction).

antenna. However, multiple antennas cannot be equipped at the position of UCA due to the half length distance restriction. The OEM communications can significantly increase the SE as compared with the traditional massive-MIMO communications. For fixed r_1, r_2, U, and N, we can obtain the wavelength region for applying the OEM communications as follows:

$$4r_2 \sin\left(\frac{\pi}{U}\right) \leq \lambda < 4r_1 \sin\left(\frac{\pi}{N}\right). \quad (54)$$

Scenario II: $d_a(r_1, N) > \lambda/2$ and $d_e(r_2, U) > \lambda/2$. In this case, we do not need to use OEM communications since the traditional massive-MIMO has achieved the maximum SE.

IV. PERFORMANCE EVALUATIONS
In this section, we evaluate the performance of our designed parabolic antenna converging and developed OEM-water-filling power allocation policy for achieving the maximum multiplicative SE in OEM communications. Throughout our evaluations, we set the frequency of carriers as 35 GHz and the angle φ as 30°. We also set $L_E = 2.947\ mm$, $L_F = 1.912\ mm$, and $W_I = 3.388\ mm$. We use HFSS to evaluate the converging and MATLAB to evaluate the multiplicative SE, respectively. The circular array consists of sixteen identical rectangular patches (array-element), which are excited by coaxial feed method [28]. The UCA is designed using F4B substrate with a relative permittivity of 2.2 and a thickness of 0.245 mm [28]. We also set $G = 36$ dB, $\eta = 50\%$, and $k = 0.4$, respectively.

Using HFSS, we evaluate the design for the UCA antenna and the parabolic antenna. The results obtained verify that the OAM signals are divergent when transmitted by the UCA

antenna and convergent after using the parabolic antenna. The obtained MATLAB results prove that OEM communications can obtain the multiplicative SE.

Figure 5 shows the directional diagrams of different OAM-modes ($l = 0, 1, 2, 3$) for non-convergent and convergent OEM waves with $N = 1$ and $M = 1$, where we set $U = V = 16$. As we expected, the maximum gain of non-convergent OEM wave decreases as the OAM-mode number increases. The array mainly radiates along the z-axis direction without a central hollow when mode number $l = 0$. This is because the OAM wave with $l = 0$ is the traditional PE wave. The central hollow becomes larger and larger as the order of OAM increases. The radius of central hollow is significantly reduced for the convergent OAM waves and the radiated power concentrates on the main lobe with little power allocated on the side lobe after converging. Figure 6 shows the unconverged and converged OAM beams for OAM-modes 0, 1, 2, and 3. OAM beams are reflected by the parabolic antenna.

Figure 7 depicts our developed OEM-water-filling power allocation policy versus the instantaneous channel SNR in OEM communications, where we set $N = M = 8$ ($U = V = 2$), $N = M = 16$ ($U = V = 4$), and $N = M = 32$ ($U = V = 8$), respectively. The average transmit power is given by $\overline{P} = 0.2$ W. As shown in Fig. 7 before converging, the allocated power severely decreases as the order of OAM increases. There is little power allocated to the high order OAM-modes in OEM communications. This is because the average received SNRs on high order of OAM-modes are very small, which is consistent with the property of Bessel functions. After converging, almost all OAM-modes can be allocated part of power. Thus, for U array-elements,
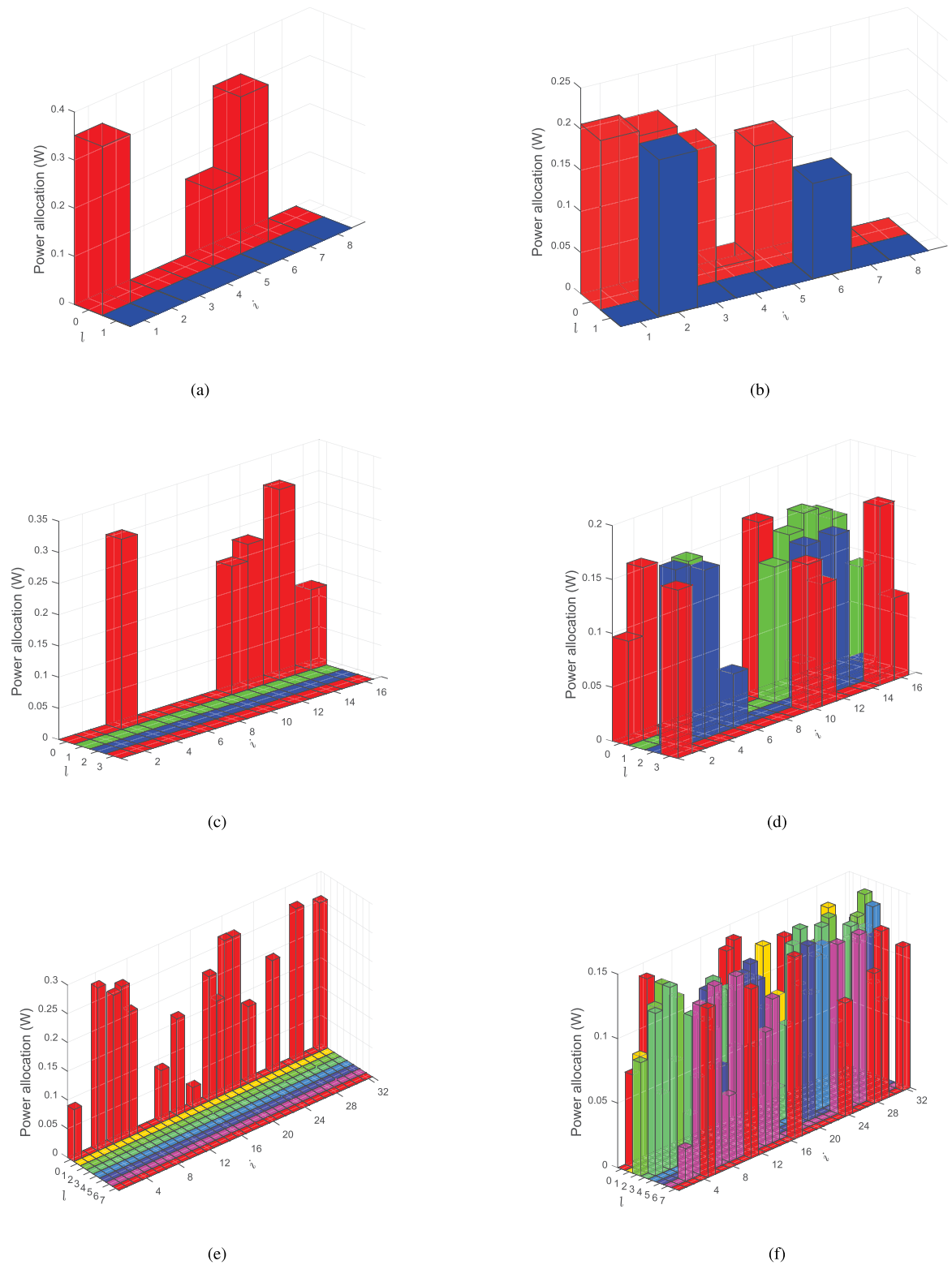
FIGURE 7. The three cases of instantaneous OEM-water-filling power allocations for non-convergent and convergent OEM communications. (a) Non-convergent OEM, $N = M = 8(U = V = 2)$. (b) Convergent OEM, $N = M = 8(U = V = 2)$. (c) Non-convergent OEM, $N = M = 16(U = V = 4)$. (d) Convergent OEM, $N = M = 16(U = V = 4)$. (e) Non-convergent OEM, $N = M = 32(U = V = 8)$. (f) Convergent OEM, $N = M = 32(U = V = 8)$.
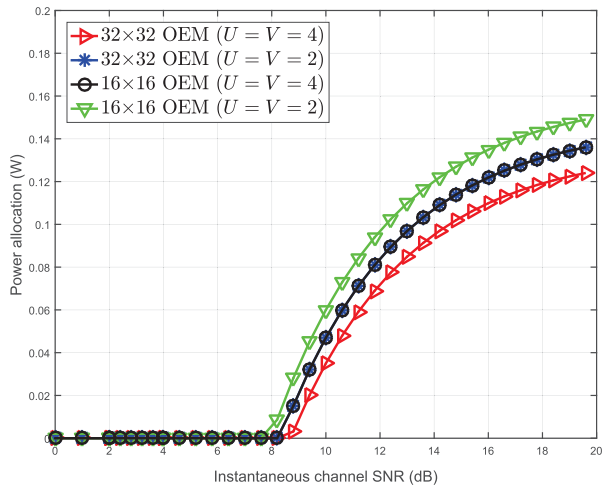
FIGURE 8. The OEM-water-filling power allocation versus instantaneous channel SNR.
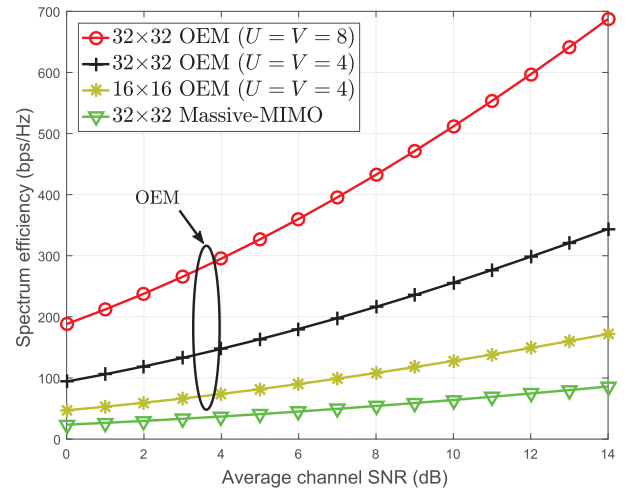
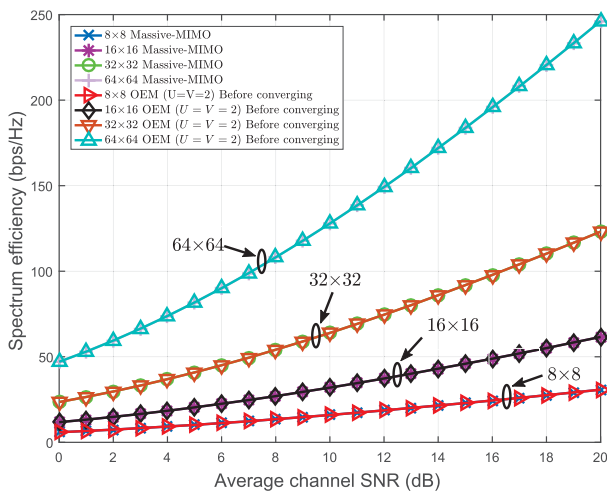**FIGURE 10.** The average spectrum-efficiency versus the average channel SNR.

FIGURE 9. The average spectrum-efficiencies of non-convergent OEM and traditional massive-MIMO.

the generated U OAM modes can be used to increase the SE for OEM communications.

Figure 8 shows our developed OEM-water-filling power allocation versus the instantaneous received channel SNR, where we set $N = M = 32$ ($U = V = 4$ and $U = V = 2$, respectively) and $N = M = 16$ ($U = V = 4$ and $U = V = 2$, respectively) for OEM communications. As shown in Fig. 8, the power allocation of OEM-water-filling policy increases as the instantaneous channel received SNR increases until reaching to a maximum value and holds on. The allocated power for $U = V = 4$ OEM communications is less than that for corresponding $U = V = 2$ OEM comminations. This is because the power is generally averaged allocated to different OAM-modes. The allocated power for $N = M = 32$ ($U = V = 2$) OEM communications and $N = M = 16$ ($U = V = 4$) OEM communications are the same. This is because both of them have the same number of orthogonal channels.

Figure 9 depicts the average SEs of non-convergent OEM communications and traditional massive-MIMO communications, where we set $U = V = 2$ and $M = N = 8$, 16, 32, and 64, respectively. Observing the curves in Fig. 9, all SEs for non-convergent OEM and traditional massive-MIMO increase as the average channel SNR increases. More importantly, when equipping with the same transmit-UCAs and receive-UCAs, the non-convergent OEM and the traditional massive-MIMO obtain the same SE, as verified for $M = N = 8$, 16, 32, and 64 cases in Fig. 9. The reason why the SEs of non-convergent OEM and traditional massive-MIMO are the same is that much power is allocated to the low order OAM-mode while the high order OAM-mode is allocated almost zero power. Therefore, it is necessary to converge OEM waves to efficiently use the high order OAM-mode to achieve maximum SE for OEM communications.

Figure 10 compares the average SEs of convergent OEM and traditional massive-MIMO communications, where we set $N = M = 32$ ($U = V = 8$ and $U = V = 4$, respectively) for OEM communication, $N = M = 16$ ($U = V = 4$) for OEM communication, and $N = M = 32$ for massive-MIMO communication, respectively. As shown in Fig. 10, the OEM communications significantly increase average SEs as compared with the traditional massive-MIMO communications. The $N = M = 16$ ($U = V = 4$), $N = M = 32$ ($U = V = 4$), and $N = M = 32$ ($U = V = 8$) OEM communications achieve double, 4 times, 8 times SEs, respectively, as compared with the $N = M = 32$ massive-MIMO communication. This is because the OEM communication can obtain not only the SE of traditional massive-MIMO communication, but also the SE of embedded OAM communication. The joint OAM and MIMO communications offers the multiplicative SE which is the SE of traditional massive-MIMO communication times the SE of embedded OAM communication.

V. CONCLUSIONS

We proposed the framework for OEM communications to obtain multiplicative spectrum-efficiency gains for joint OAM and massive-MIMO mmWave wireless communications. We designed the parabolic antenna to converge the OAM waves. Then, we developed the joint mode-decomposition and multiplexing-detection scheme to decompose and detect the transmit signal on each OAM-mode of each transmit UCA antenna. We also developed the OEM-water-filling power allocation policy to achieve the maximum multiplicative spectrum-efficiency for OEM communications. The simulation results validated the parabolic antenna based converging, the joint mode-decomposition and multiplexing-detection scheme, and the OEM-water-filling policy. The OEM communications can obtain the multiplicative spectrum-efficiency gain for joint OAM and massive-MIMO communications, thus achieving much larger spectrum-efficiency than the traditional massive-MIMO mmWave communications.

REFERENCES

[1] J. G. Andrews *et al.*, "What will 5G be?" *IEEE J. Sel. Areas Commun.*, vol. 32, no. 6, pp. 1065–1082, Jun. 2014.

[2] T. Bai, A. Alkhateeb, and R. W. Heath, "Coverage and capacity of millimeter-wave cellular networks," *IEEE Commun. Mag.*, vol. 52, no. 9, pp. 70–77, Sep. 2014.

[3] E. G. Larsson, O. Edfors, F. Tufvesson, and T. L. Marzetta, "Massive MIMO for next generation wireless systems," *IEEE Commun. Mag.*, vol. 52, no. 2, pp. 186–195, Feb. 2014.

[4] Z. Gao, L. Dai, D. Mi, Z. Wang, M. A. Imran, and M. Z. Shakir, "MmWave massive-MIMO-based wireless backhaul for the 5G ultra-dense network," *IEEE Wireless Commun.*, vol. 22, no. 5, pp. 13–21, Oct. 2015.

[5] M. Dohler, R. W. Heath, A. Lozano, C. B. Papadias, and R. B. Valenzuela, "Is the PHY layer dead?" *IEEE Commun. Mag.*, vol. 49, no. 4, pp. 159–165, Apr. 2011.

[6] *International Mobile Telecommunications 2020*. Accessed: 2015. [Online]. Available: http://www.itu.int/en/ITU-T/focusgroups/imt-2020/Pages/default.aspx

[7] B. Thidé *et al.*, "Utilization of photon orbital angular momentum in the low-frequency radio domain," *Phys. Rev. Lett.*, vol. 99, no. 8, pp. 087701-1–087701-4, Aug. 2007.

[8] K. A. Opare, Y. Kuang, J. J. Kponyo, K. S. Nwizege, and Z. Enzhan, "The degrees of freedom in wireless line-of-sight oam multiplexing systems using a circular array of receiving antennas," in *Proc. 5th Int. Conf. Adv. Comput. Commun. Technol.*, Feb. 2015, pp. 608–613.

[9] K. A. Opare and Y. Kuang, "Performance of an ideal wireless orbital angular momentum communication system using multiple-input multiple-output techniques," in *Proc. Int. Conf. Telecommun. Multimedia (TEMU)*, Jul. 2014, pp. 144–149.

[10] O. Edfors and A. J. Johansson, "Is orbital angular momentum (OAM) based radio communication an unexploited area?" *IEEE Trans. Antennas Propag.*, vol. 60, no. 2, pp. 1126–1131, Feb. 2012.

[11] M. Tamagnone, J. S. Silva, S. Capdevila, J. R. Mosig, and J. Perruisseau-Carrier, "The orbital angular momentum (OAM) multiplexing controversy: OAM as a subset of MIMO," in *Proc. 9th Eur. Conf. Antennas Propag. (EuCAP)*, Apr. 2015, pp. 1–5.

[12] K. A. Opare, Y. Kuang, and J. J. Kponyo, "Mode combination in an ideal wireless OAM-MIMO multiplexing system," *IEEE Wireless Commun. Lett.*, vol. 4, no. 4, pp. 449–452, Aug. 2015.

[13] Q. Bai, A. Tennant, and B. Allen, "Experimental circular phased array for generating OAM radio beams," *Electron. Lett.*, vol. 50, no. 20, pp. 1414–1415, Sep. 2014.

[14] B. Allen, A. Tennant, Q. Bai, and E. Chatziantoniou, "Wireless data encoding and decoding using OAM modes," *Electron. Lett.*, vol. 50, no. 3, pp. 232–233, Jan. 2014.

[15] X. Hui *et al.*, "Ultralow reflectivity spiral phase plate for generation of millimeter-wave OAM beam," *IEEE Antennas Wireless Propag. Lett.*, vol. 14, pp. 966–969, 2015.

[16] A. Cagliero, A. De Vita, R. Gaffoglio, and B. Sacco, "A new approach to the link budget concept for an OAM communication link," *IEEE Antennas Wireless Propag. Lett.*, vol. 15, pp. 568–571, 2016.

[17] K. Liu *et al.*, "Generation of OAM beams using phased array in the microwave band," *IEEE Trans. Antennas Propag.*, vol. 64, no. 9, pp. 3850–3857, Sep. 2016.

[18] Y. Chen *et al.*, "A flat-lensed spiral phase plate based on phase-shifting surface for generation of millimeter-wave OAM beam," *IEEE Antennas Wireless Propag. Lett.*, vol. 15, pp. 1156–1158, 2016.

[19] W. Cheng, X. Zhang, and H. Zhang, "QoS-aware power allocations for maximizing effective capacity over virtual-MIMO wireless networks," *IEEE J. Sel. Areas Commun.*, vol. 31, no. 10, pp. 2043–2057, Oct. 2013.

[20] M. Yousefbeiki and J. Perruisseau-Carrier, "Towards compact and frequency-tunable antenna solutions for MIMO transmission with a single RF chain," *IEEE Trans. Antennas Propag.*, vol. 62, no. 3, pp. 1065–1073, Mar. 2014.

[21] M. Cheng, L. Guo, J. Li, S. Liu, and M. Cheng, "Effects of atmospheric turbulence on mode purity of orbital angular momentum millimeter waves," in *Proc. IEEE Int. Symp. Antennas Propag. USNC/URSI Nat. Radio Sci. Meeting*, Jul. 2017, pp. 1845–1846.

[22] Y. Yan *et al.*, "OFDM over mm-wave OAM channels in a multipath environment with intersymbol interference," in *Proc. IEEE Global Commun. Conf. (GLOBECOM)*, Dec. 2016, pp. 1–6.

[23] M. Oldoni *et al.*, "Space-division demultiplexing in orbital-angular-momentum-based MIMO radio systems," *IEEE Trans. Antennas Propag.*, vol. 63, no. 10, pp. 4582–4587, Oct. 2015.

[24] Z. Zhang, S. Zheng, W. Zhang, X. Jin, H. Chi, and X. Zhang, "Experimental demonstration of the capacity gain of plane spiral OAM-based MIMO system," *IEEE Microw. Wireless Compon. Lett.*, vol. 27, no. 8, pp. 757–759, Aug. 2017.

[25] K. Murata, N. Honma, K. Nishimori, N. Michishita, and H. Morishita, "Analog eigenmode transmission for short-range MIMO based on orbital angular momentum," *IEEE Trans. Antennas Propag.*, vol. 65, no. 12, pp. 6687–6702, Dec. 2017.

[26] B. Thidé, *Electromagnetic Field Theory*, 2nd ed. Mineola, NY, USA: Dover, 2011.

[27] S. Gao, W. Cheng, H. Zhang, and Z. Li, "High-efficient beam-converging for UCA based radio vortex wireless communications," in *Proc. IEEE/CIC Int. Conf. Commun. China (ICCC)*, Qingdao, China, Oct. 2017, pp. 1–6.

[28] I. J. Bahl and P. Bhartia, *Microstrip Antennas*. Norwood, MA, USA: Artech House, 1980.

[29] I. J. Bahl, P. Bhartia, and S. S. Stuchly, "Design of microstrip antennas covered with a dielectric layer," *IEEE Trans. Antennas Propag.*, vol. 30, no. 2, pp. 314–318, Mar. 1982.

[30] R. D. Javor, X.-D. Wu, and K. Chang, "Design and performance of a microstrip reflectarray antenna," *IEEE Trans. Antennas Propag.*, vol. 43, no. 9, pp. 932–939, Sep. 1995.

[31] Q. Zhu, T. Jiang, Y. Cao, K. Luo, and N. Zhou, "Radio vortex for future wireless broadband communications with high capacity," *IEEE Wireless Commun.*, vol. 22, no. 6, pp. 98–104, Dec. 2015.

[32] Y. Yuan, Z. Zhang, J. Cang, H. Wu, and C. Zhong, "Capacity analysis of UCA-based OAM multiplexing communication system," in *Proc. Int. Conf. Wireless Commun. Signal Process. (WCSP)*, Oct. 2015, pp. 1–5.

[33] N. M. Temme, *Special Functions: An Introduction to the Classical Functions of Mathematical Physics*. New York, NY, USA: Wiley, 1996.

[34] Y. Yan *et al.*, "High-capacity millimetre-wave communications with orbital angular momentum multiplexing," *Nature Commun.*, vol. 5, p. 4876, Sep. 2014.

[35] B. S. Guru and H. R. Hiziroglu, *Electromagnetic Field Theory Fundamentals*. Cambridge, U.K.: Cambridge Univ. Press, 2009.

[36] H. R. Anderson, *Fixed Broadband Wireless System Design*. New York, NY, USA: Wiley, 2003.

[37] R. D. Oliveira and M. Helier, "Closed-form expressions of the axial step and impulse responses of a parabolic reflector antenna," *IEEE Trans. Antennas Propag.*, vol. 55, no. 4, pp. 1030–1037, Apr. 2007.

[38] S. Boyd and L. Vandenberghe, *Convex Optimization*. Cambridge, U.K.: Cambridge Univ. Press, 2004.

[39] A. J. Goldsmith, *Wireless Communications*. Cambridge, U.K.: Cambridge Univ. Press, 2005.

[40] D. Tse and P. Viswanath, *Fundamentals of Wireless Communication*. Cambridge, U.K.: Cambridge Univ. Press, 2005.

[41] A. J. Paulraj, D. A. Gore, R. U. Nabar, and H. Bolcskei, "An overview of MIMO communications—A key to gigabit wireless," *Proc. IEEE*, vol. 92, no. 2, pp. 198–218, Feb. 2004.

WENCHI CHENG (M'14) received the B.S. and Ph.D. degrees in telecommunication engineering from Xidian University, China, in 2008 and 2014, respectively. He was a Visiting Scholar at the Networking and Information Systems Laboratory, Department of Electrical and Computer Engineering, Texas A&M University, College Station, TX, USA, from 2010 to 2011. He joined the Department of Telecommunication Engineering, Xidian University, in 2013, as an Assistant Professor. He is currently an Associate Professor with Xidian University. He has published over 50 international journals and conference papers, including the IEEE JOURNAL ON SELECTED AREAS IN COMMUNICATIONS, IEEE Magazines, IEEE Transactions, and the IEEE INFOCOM, GLOBECOM, and ICC. His current research interests include 5G wireless networks and orbital-angular-momentum-based wireless communications. He has served or serving as a TPC Member for INFOCOM, GLOBECOM, and ICC. He has served or serving as the ICC 2019 Publicity Chair. He received the Young Elite Scientist Award of CAST, the Best Dissertation (Rank 1) of the China Institute of Communications, the Best Paper Nomination for the IEEE GLOBECOM 2014, and the Outstanding Contribution Award for Xidian University. He has served or serving as an Associate Editor for the IEEE ACCESS.

HAILIN ZHANG (M'97) received the B.S. and M.S. degrees from Northwestern Polytechnic University, Xi'an, China, in 1985 and 1988, respectively, and the Ph.D. degree from Xidian University, Xi'an, in 1991. In 1991, he joined the School of Telecommunications Engineering, Xidian University, where he is currently a Senior Professor and the Dean of the School of Telecommunications Engineering. He is also the Director of the Key Laboratory in Wireless Communications Sponsored by the China Ministry of Information Technology, a Key Member of the State Key Laboratory of Integrated Services Networks, one of the state government specially compensated scientists and engineers, the Field Leader in telecommunications and information systems with Xidian University, and an Associate Director of the National 111 Project. He has published over 300 papers in journals and conferences. His current research interests include key transmission technologies and standards on broadband wireless communications for 5G and 5G-beyond wireless access systems.

LIPING LIANG received the B.S. degree in electronic and information engineering from Jilin University, Changchun, China, in 2015. She is currently pursuing the Ph.D. degree in communication and information system with Xidian University, Xi'an, China. Her research interests focus on 5G wireless communications with emphasis on vortex wireless communications and anti-jamming communications.

HAIYUE JING is currently pursuing the Ph.D. degree in communication engineering with Xidian University, Xian, China. His research interests focus on the generation of orbital-angular-momentum waves, mode-detection schemes, and high capacity of radio vortex wireless communications.

ZAN LI (SM'14) received the B.S. degree in communications engineering in 1998, and the M.S. and Ph.D. degrees in communication and information systems from Xidian University, Xi'an, China, in 2001 and 2004, respectively. She is currently a Professor with the State Key Laboratory of Integrated Services Networks, School of Telecommunications Engineering, Xidian University. Her research interests include topics on wireless communications and signal processing, such as weak signal detection, spectrum sensing, and cooperative communications.

• • •